Proceedings of the ASME 2014 International Mechanical Engineering Congress and Exposition
IMECE2014
November 14-20, 2014, Montreal, Quebec, Canada

IMECE2014-39354

ON THE VORTEX BREAKDOWN PHENOMENON IN HIGH ANGLE OF ATTACK FLOWS OVER DELTA WING GEOMETRIES

Eric D. Robertson
Mississippi State University
Department of Mechanical Engineering
Starkville, MS, USA

Varun Chitta
Mississippi State University
Department of Mechanical Engineering
Starkville, MS, USA

D. Keith Walters
Mississippi State University
Department of Mechanical Engineering
Starkville, MS, USA

Shanti Bhushan
Mississippi State University
Center for Advanced Vehicular Systems
Starkville, MS, USA

ABSTRACT

Using computational methods, an investigation was performed on the physical mechanisms leading to vortex breakdown in high angle of attack flows over delta wing geometries. For this purpose, the Second International Vortex Flow Experiment (VFE-2) 65° sweep delta wing model was studied at a root chord Reynolds number (Re_{cr}) of 6×10^6 at various angles of attack. The open-source computational fluid dynamics (CFD) solver OpenFOAM was used in parallel with the commercial CFD solver ANSYS® FLUENT. For breadth, a variety of classic closure models were applied, including unsteady Reynolds-averaged Navier-Stokes (URANS) and detached eddy simulation (DES). Results for all cases are analyzed and flow features are identified and discussed. The results show the inception of a pair of leading edge vortices originating at the apex for all models used, and a region of steady vortical structures downstream in the URANS results. However, DES results show regions of massively separated helical flow which manifests after vortex breakdown. Analysis of turbulence quantities in the breakdown region gives further insight into the mechanisms leading to such phenomena.

NOMENCLATURE

α	Flow angle of attack
b	Wingspan at particular station, m
c_r	Root chord length, m
η	Spanwise location, x/b
k	Turbulence Kinetic Energy, kg m^2 / s^2
ν	Kinematic viscosity, Pa-s
ν_T	Turbulent kinematic viscosity, Pa-s
ω	Specific Dissipation Rate, 1/s
Ω	Vorticity, 1/s
Re_{cr}	Reynolds number at root chord
Ti	Turbulence Intensity, %
u_∞	Freestream velocity, m/s
ξ	Streamwise station number, x/c_r
y^+	Non-dimensional first cell height

INTRODUCTION

Wings with delta shape are commonly used in high-performance aircraft as a means of increasing maneuverability. At high angles of attack, the boundary layer detaches from the surface and is accompanied by the formation of a pair of steady conical vortices. These vortices, which originate at the apex of the wing in sharp leading edge configurations [1], create strong regions of low pressure on the surface of the wing. These regions of low pressure, due to high flow velocities very near the wing surface, induce an extra component of lift. This extra component, often called vortex lift [1-2], in turn increases maneuverability (mainly by increasing the stall angle of attack). An added consequence is a huge increase in drag, which is directly attributable to the large regions of low pressure that exist in the vortex core. An increase in angle of attack leads to the unsteady phenomenon of vortex breakdown, generally observed over the rear portion of the wing. This is characterized by a complete destruction of the steady vortices that stream down the body of the wing. This phenomenon can not only significantly affect the stability and aerodynamic characteristics of the aircraft as a

whole, but may also heighten structural fatigue (due to vibrations and strong fluctuations in pressure).

One of the earliest studies on vortex breakdown was recorded in literature by Werlé in 1954 [3], who visualized and observed the phenomenon in a water tunnel. These results were first validated by Peckham and Atkinson [4] and then by Elle [5]. Since, numerous experimental, theoretical, and numerical studies have been conducted in pursuit of enhanced understanding of the physics surrounding vortical flow, breakdown, and their control. Notably, Benjamin [6-7] and Leibovich [8] have contributed a great deal, chiefly by narrating in detail the character of and theories behind breakdown.

Recently, numerical and experimental studies performed by participants of the Second International Vortex Flow Experiment (Project VFE-2) [9-11] have demonstrated the robustness of the full viscous Navier–Stokes equations in accurately resolving the flow field around a delta wing geometry. These studies aimed to examine the effects of Mach number, Reynolds number, angle of attack, and leading edge bluntness, but were generally limited to observations based on pressure and aerodynamic coefficient predictions [12]. Furman [10] provided insight on the mechanisms of turbulence in the breakdown region using physical experiments, particularly through observation of the turbulent stresses and pressure fluctuations. More recently, a study by Cummings and Schutte [11] investigated flows around delta wings using Detached-Eddy Simulation (DES). The present investigation aims to conduct similar studies, particularly in pursuit of an enhanced understanding of the characteristics of turbulence and turbulence modelling in the breakdown region.

GEOMETRY

The 65° sweep delta wing (without sting) used in this study has been derived from the dimensions of the geometry used in the aforementioned VFE-2 experiment. Only the sharp leading edge geometry is used. The dimensions of the geometry are shown in Figure 1.

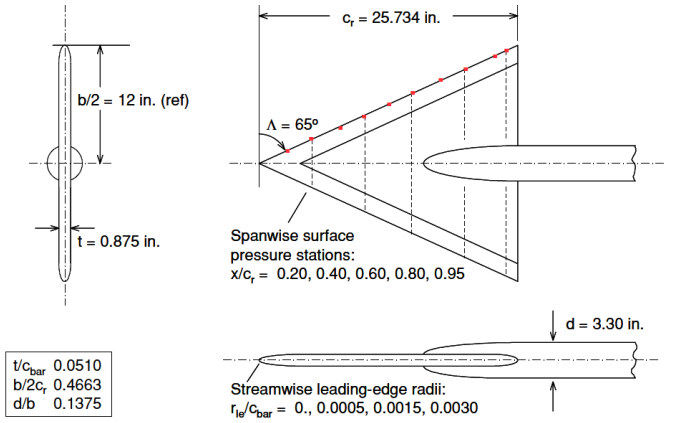

Fig. 1 Geometry of delta wing [1]. The present computational study excludes the sting.

GRID GENERATION

Two volume grids (4M and 7M cells) were generated using an in-house grid generation software, SolidMesh [13]. Both grids feature a body-fitted layer of structured cells accompanied by unstructured tetrahedral in the freestream. The near-wall value of $y^+ < 1$ is enforced to adequately resolve the viscous sub-layer.

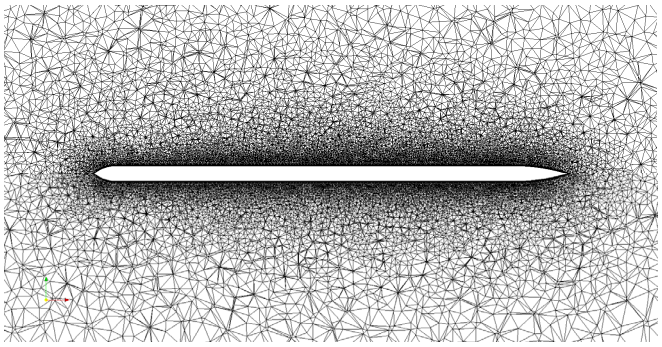

Fig. 2 Computational mesh at root chord plane.

NUMERICAL METHOD

The governing equations utilized in this numerical study are the incompressible three–dimensional Navier–Stokes (N-S) equations in finite volume formulation, as shown by Eqn. (1).

$$\frac{\partial u_i}{\partial t} + u_j \frac{\partial u_i}{\partial x_j} = -\frac{1}{\rho}\frac{\partial p}{\partial x_i} + \nu \frac{\partial^2 u_i}{\partial x_j \partial x_j} - \frac{\partial \tau_{ij}}{\partial x_j} \qquad (1)$$

The incompressible assumption is valid in low-speed regimes of flight, such as takeoff and landing, where compressibility effects are negligible. Incidentally, these flight regimes are also associated with the angles of attack studied in this work.

As previously mentioned, the main interest of this study is to observe the character of turbulence. As such, the concern is with producing high-fidelity results using various closure models with minimal regard to computational cost. Modelling of the turbulent stresses τ_{ij} is accomplished using URANS (k-ω SST [14]) and a hybrid RANS-LES model (SA-DDES [15]) These models were chosen for their strengths in predicting flows with strong adverse pressure gradients (k-ω SST) and ability to resolve large–scale flow features without requiring an unreasonably fine computational mesh (SA-DDES).

The OpenFOAM [21] computational toolbox is a free, open-source software package capable of simulating a wide variety of fluid flow processes. The default software includes over 80 solver modules, each tailored to flows ranging from simple incompressible and compressible flows to chemical reactions and fluid-structure interactions. For further details about the numerical methods and algorithms available in OpenFOAM, the user should consult [22].

Shear Stress Transport Model

The *k-ω* SST model is a basic two-equation eddy viscosity model. SST utilizes the standard *k-ω* model in near wall regions and *k-ε* in the freestream. This is to take advantage of the strengths of standard *k-ω* in strong adverse pressure gradients, and covers the weakness of *k-ε* with regard to meshes with $y^+ < 1$. The transport equations for turbulence kinetic energy (*k*) and specific dissipation rate (ω) are shown.

$$\frac{\partial k}{\partial t} + u_i \frac{\partial k}{\partial x_j} = \tilde{P}_k - \beta^* k\omega + \frac{\partial}{\partial x_i}\left[(\nu + \sigma_k \nu_T)\frac{\partial k}{\partial x_i}\right] \quad (2)$$

$$\frac{\partial \omega}{\partial t} + u_i \frac{\partial \omega}{\partial x_j} = \alpha S^2 - \beta \omega^2 + \frac{\partial}{\partial x_i}\left[(\nu + \sigma_\omega \nu_T)\frac{\partial \omega}{\partial x_i}\right] + 2(1 - F_1)\sigma_{\omega 2}\frac{1}{\omega}\frac{\partial k}{\partial x_i}\frac{\partial \omega}{\partial x_i} \quad (3)$$

Further details regarding model coefficients are given in [14]. The eddy viscosity is defined from the solutions to the above transport equations, i.e.,

$$\nu_T = \frac{a_1 k}{\max(a_1 \omega, SF_2)} \quad (4)$$

The terms F_1 and F_2 serve as blending functions, which facilitate the usage of either *k-ω* or *k-ε*.

$$F_1 = tanh\left\{\left\{\min\left[\max\left(\frac{\sqrt{k}}{\beta^* \omega y}, \frac{500\nu}{y^2 \omega}\right), \frac{4\sigma_{\omega 2} k}{CD_{k\omega} y^2}\right]\right\}^4\right\} \quad (5)$$

$$F_2 = tanh\left[\left[\max\left(\frac{2\sqrt{k}}{\beta^* \omega y}, \frac{500\nu}{y^2 \omega}\right)\right]^2\right] \quad (6)$$

Spalart-Allmaras DDES Methodology

The base Spalart-Allmaras one-equation turbulence model involves the transport of a modified turbulent viscosity, $\tilde{\nu}$, which is obtained through the solution of the following transport equation.

$$\frac{\partial \tilde{\nu}}{\partial t} + u_j \frac{\partial \tilde{\nu}}{\partial x_j} = \frac{1}{\sigma}\frac{\partial}{\partial x_k}\left[(\nu + \tilde{\nu})\frac{\partial}{\partial x_k}\right] + c_{b1}\tilde{S}\tilde{\nu} - c_{w1} f_w \left(\frac{\tilde{\nu}}{d}\right)^2 + \frac{c_{b2}}{\sigma}\frac{\partial \tilde{\nu}}{\partial x_k}\frac{\partial \tilde{\nu}}{\partial x_k} \quad (7)$$

Details behind the various closure coefficients and terms are given in [16]. The turbulent viscosity is given as directly proportional (by the constant f_{v1}) to the solution to the transport equation, i.e.,

$$\nu_T = \tilde{\nu} f_{v1} \quad (8)$$

The DDES approach takes the length scale d in Eqn. (7) and replaces it with a modified length scale, given by Eqn. (9). This formulation applies a RANS-like treatment to near-wall regions and an LES-like treatment elsewhere.

$$\tilde{d} = d - f_d \max[0, d - C_{DES}\Delta] \quad (9)$$

The term f_d is a blending factor which delineates between boundary layer and freestream regions (further explained in [15]). A value of $f_d = 0$ renders $\tilde{d} = d$ (RANS), while $f_d = 1$ activates LES content. By default, the constant $C_{DES} = 0.65$, though some [17-18] have studied the effect of tuning this term for better results. The present investigation uses the default value. The term Δ is simply the largest dimension of a particular computational cell.

Numerical Schemes

A 2nd order linear convection scheme with limiting is used in order to minimize the influence of numerical dissipation on the resolution of flow structures. In OpenFOAM, this corresponds to the user setting *limitedLinear*, which is central differencing bounded with a variation of the Sweby limiter ($\Psi(r)$) [19].

$$\phi_f = \phi_{f_{UD}} + \Psi(r)\left(\phi_{f_{HO}} - \phi_{f_{UD}}\right) \quad (10)$$

$$\Psi(r) = \max\left(min\left(\frac{2}{K}r, 1\right), 0\right) \quad (11)$$

The OpenFOAM limiter, given by Eqn. (11), is centered on a user-defined setting *K*, where $0 \leq K \leq 1$. A setting of $K = 1$ reduces the method to 1st order in the presence of high gradients (thus, improving the stability of the central difference), while $K = 0$ corresponds to minimal limiting. The present study uses the setting $K = 0.5$ to preserve the accuracy of the method while introducing stability.

Temporal terms are discretized using a three-point backward scheme, while transport equations of turbulence were differenced using the 2nd order upwind scheme.

Boundary Conditions

Far field inflow boundaries are prescribed with a freestream velocity of $u = 1$ at three different angles of attack (18, 23, and 65°). The kinematic viscosity is adjusted to a flow condition of $Re_{cr} = 6 \times 10^6$. Freestream turbulence intensity is set to Ti = 0.05%.

Solution Algorithm

For pressure–velocity coupling, the PISO algorithm [20], a typical predictor-corrector method which solves the pressure field using a Poisson equation, is used. In OpenFOAM, this method is present in the *pimpleFOAM* solver and is the central part of the *pisoFOAM* and other transient N-S solvers carrying the *piso-* name. For time accuracy, a maximum convective CFL = 1 is used.

RESULTS

A comparison to available experimental data is given, along with qualitative observations about the physics of the flow field. For the sake of validation, OpenFOAM results are compared against FLUENT results. Predicted pressure and vorticity data are among the data sets that are quantitatively assessed. For vortex visualization, the Q-criterion [23] is used. Each case setup is, from here on, referred to as follows: SA-DDES model on 4M grid (DDES-4M), on 7M grid (DDES-7M); and SST model on 4M grid (SST-4M). The suffix –OF and –FL denote results from OpenFOAM and FLUENT, respectively.

Overall Flow Physics

Qualitative results from both grids and models show a vibrant picture of two primary vortices originating at the apex of the wing. OpenFOAM predictions show that SA-DDES shows the clearest picture of the character of breakdown, predicting a bubble-like structure before descending into a spiral burst mode. DDES-4M-OF shows a less discernible breakdown bubble and weaker instability than DDES-7M-OF (Fig. 3(a,b)).

SST-URANS appears to only faintly predict the breakdown phenomenon. SST-4M-OF (Fig. 3(c)) predicts the bubble structure at the rear of the wing and begins to show changes in axial vorticity in the core, but fails to show any indication of spiral burst. Because of this, most of the following observations are made from the SA-DDES model.

FLUENT fails to predict any element of breakdown at all (Fig. 3(e,f)). A closer inspection reveals DDES-4M-FL shows a turbulent viscosity in the vortex core of up to 100 times greater than OpenFOAM predictions. This acts against the role of the mechanisms of turbulence in generating breakdown and such results warrant future studies.

Mechanisms of Breakdown and Spiral Burst Mode

The inception of the bubble-like structure is associated with a sharp decrease in axial momentum and increase in pressure. This is consistent with the "stagnation point" observation made by Leibovich [8] and lends credence to a notion that the adverse pressure gradient plays a large role in vortex burst. The bubble is followed by the onset of the spiral burst mode, which is indicated by a change in sign of axial vorticity (Ω_x) in the core (Fig. 4)- consistent with observations made by Ludwieg [24] and indicative of the full onset of breakdown [24]. FLUENT results do not show this change in sign of axial vorticity, further lending credence to the notion of it being a critical element in this phenomenon.

The full onset of breakdown is associated with the spiral burst mode and is most prominently observed at $\alpha = 23°$. This mode is characterized by large-scale helical structures, which appear to break off from the bubble. The frequency of rotation of these structures is described by a transient quasi-periodic variation in pressure at a location in the core near the onset of the instability. Shown by Fig. 6, this oscillation occurs at a frequency of approximately 2 s^{-1} (at $\xi \approx 0.55$) for $\alpha = 23°$.

Detailed observations about the physical characteristics of breakdown are as follows. Each observation parallels with station letters (a. through d.) in Fig. 4 and with station numbers (ξ) in Fig. 5.

a. ($\xi = 0$ - 0.1) Full formation of vortex, fed by shear layer roll-up from underside of wing (which begins at wing apex).
b. ($\xi = 0.50$) Full decay of axial core flow momentum and inception of bubble structure. Increased turbulent shearing stress occurs between fully decayed slow core flow and outer parts of vortex (Fig. 5(b,e)).
c. ($\xi = 0.55$) Angular direction of axial core flow has reversed and breakdown begins. Vorticity in core has changed sign. Shear layer roll-up (hook structure emanating from wing edge) continues to feed vortex. Turbulent shearing stresses continue growing, and "breakdown gap" (deficit in shearing stress, which is associated with deficit in axial vorticity in Fig. 4) can be seen (Fig. 5(c,f)).
d. ($\xi > 0.55$) Turbulent viscosity and resolved TKE surges due to increased normal stresses in vortex core. The normal stresses further evidence deformation and breakdown (stretching/elongation) of the vortex.

Breakdown Position

For a given turbulence model, the position of vortex breakdown is primarily influenced by angle of attack. By measure of the location of change in sign of Ω_x in the vortex core, the approximate breakdown locations are presented in Table 1. The flow condition at $\alpha = 23°$ first shows breakdown at $\xi \approx 0.55$, sooner than $\alpha = 18°$ ($\xi \approx 0.71$). Completely separated flow is predicted at $\alpha = 65°$, a condition associated with stall (Fig. 3(e)).

α	Case	ξ
18°	DDES-4M-OF	0.82
	DDES-7M-OF	0.71
	DDES-4M-FL	-
	SST-4M-OF	0.94
	SST-4M-FL	-
23°	DDES-7M-OF	0.55
	DDES-4M-FL	-
65°	DDES-4M-OF	imperceptible/at apex

Table 1. Approximate vortex breakdown locations.

The breakdown position tends to decrease as angle of attack increases. As the adverse pressure gradient increases with angle of attack, it is valid to conclude that an increased rate of decay in axial core flow momentum would occur and cause earlier breakdown.

It must also be noted that grid resolution has an obvious effect on breakdown location. Breakdown occurs a difference of $\xi = 0.11$ towards the apex between DDES-4M-OF and DDES-7M-OF. Future studies must include a method of grid convergence or validation.

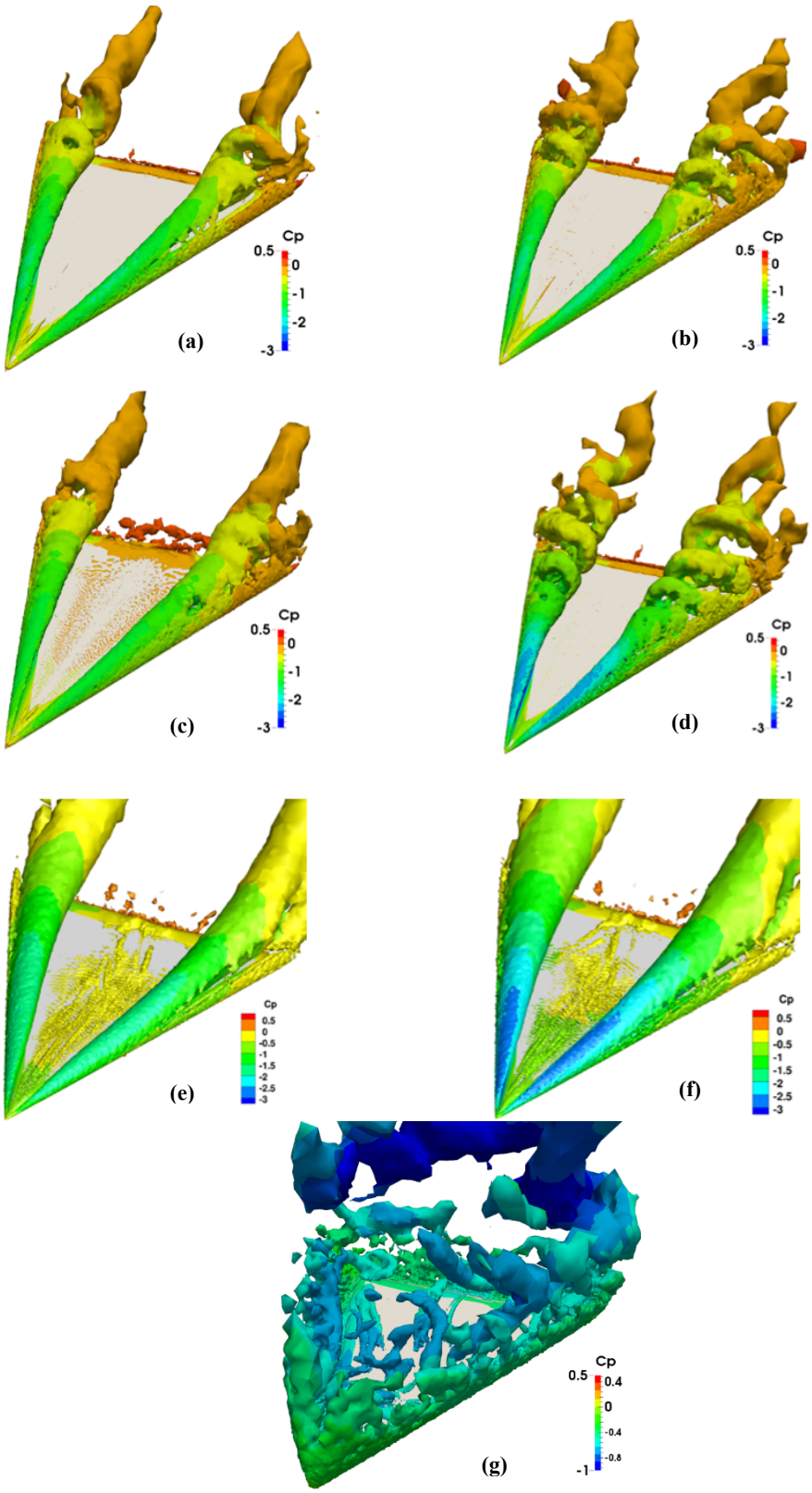

Fig. 3 Isosurfaces of $Q = 2$ contoured by pressure coefficient: (a) DDES-4M-OF $\alpha = 18°$, (b) DDES-7M-OF, $\alpha = 18°$, (c) SST-4M-OF, $\alpha = 18°$, (d) DDES-7M-OF, $\alpha = 23°$, (e) DDES-4M-FL, $\alpha = 18°$, (f) DDES-4M-FL, $\alpha = 23°$, (g) DDES-4M-OF, $\alpha = 65°$.

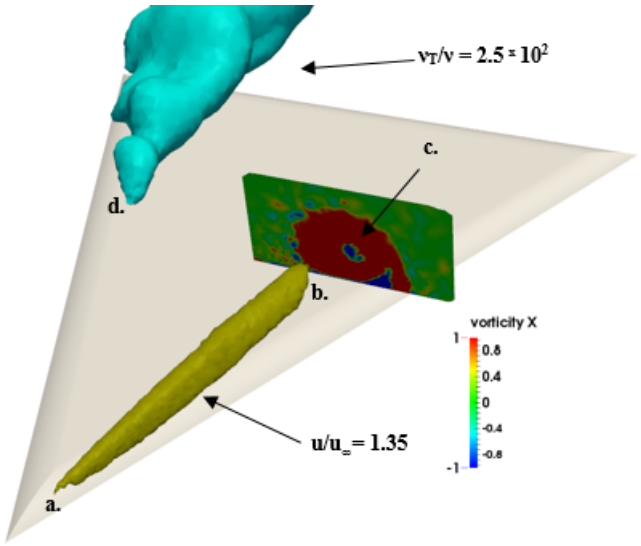

Fig. 4 Schematic demonstrating physics behind vortex breakdown for DDES-7M-OF α = 23°. Green and light-blue regions are isosurfaces of specified values.

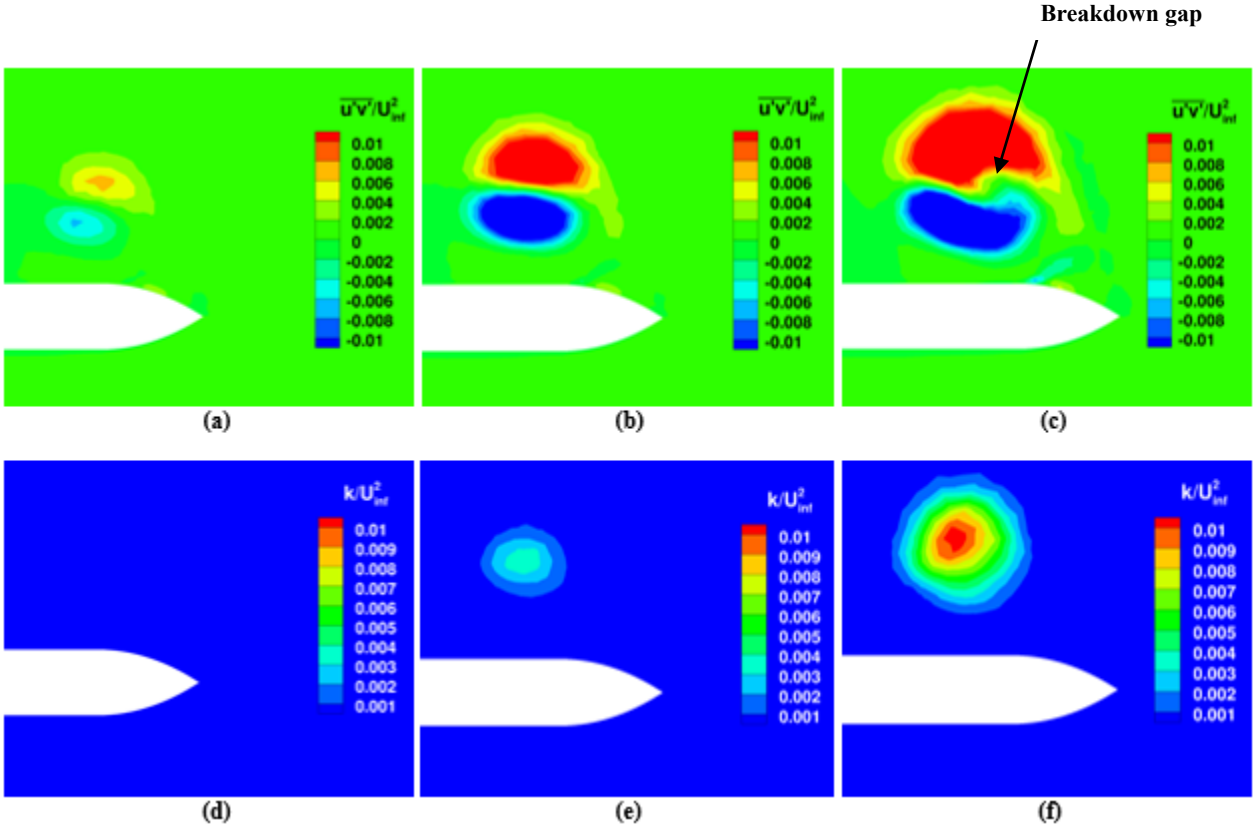

Fig. 5 Resolved mean Reynolds stress and turbulence kinetic energy in breakdown region, DDES-7M-OF α = 23°: (a) Axial-spanwise turbulent shear stress at $\xi = 0.45$, (b) at $\xi = 0.5$, and (c) at $\xi = 0.55$; (d) Resolved TKE at $\xi = 0.45$, (e) at $\xi = 0.5$, (f) at $\xi = 0.55$. The arrow indicates the position of the inception of vortex breakdown.

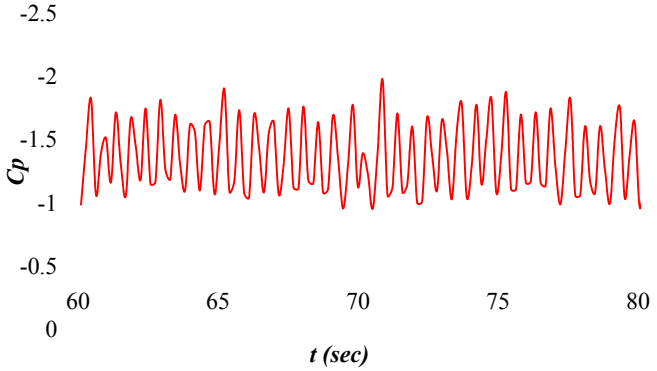

Fig. 6 Transient behavior of pressure at $\xi \approx 0.55$, vortex core, DDES-7M-OF $\alpha = 23°$.

Pressure Distribution and Rise in Core

Contours of surface pressure (Fig. 7) show distinct differences between angle of attack. A long, stratified line of low pressure is seen for $\alpha = 18°$, suggesting a more delayed onset of breakdown (consistent with previous observations).

According to [1], surface pressure distributions on sharp leading edge configurations show little dependence on Reynolds number. Therefore, the $Re = 2 \times 10^6$ results from [25] are used for surface pressure comparison with little trepidation (Fig. 8(a-e)). Each maxima corresponds to the position of the primary vortex. Forward of $\xi = 0.6$, reasonable agreement is seen. At $\xi = 0.8$ and 0.95, vast disagreement is seen, which is directly attributable to the absence of a sting in the present computational results. OpenFOAM and FLUENT show reasonable agreement with one another, with the exception of the breakdown region (Fig. 8(c-d)). Here, FLUENT under-predicts the rise in core pressure associated with the breakdown occurrence. Table 2 illustrates the progression of core pressure

Moreover, results show (Fig. 8(d-e)) that the presence of a sting in the experiment repositions the location of the vortex inward by a distance of $\eta = 0.1$-0.2. Theoretically, the sting creates a low-pressure region of flow acceleration around it, which attracts the primary vortex.

The surface pressure profiles also reveal the existence of a pair of secondary vortices, which appear to manifest aft of the apex (but before $\xi = 0.4$). This is shown by the subordinate peaks shown in Fig. 8(b-e). OpenFOAM predicts this inception between $\xi = 0.2$-0.4; FLUENT $\xi = 0.4$-0.6.

ξ	Code	Cp (averaged)
0.2	OpenFOAM	-2.26
	FLUENT	-2.27
0.4	OpenFOAM	-2.43
	FLUENT	-2.45
0.6	OpenFOAM	-1.67
	FLUENT	-2.11
0.8	OpenFOAM	-0.98
	FLUENT	-1.46

Table 2. Progression of core pressure in the primary vortex, DDES-4M, $\alpha = 18°$. Breakdown location is approximately $\xi = 0.71$.

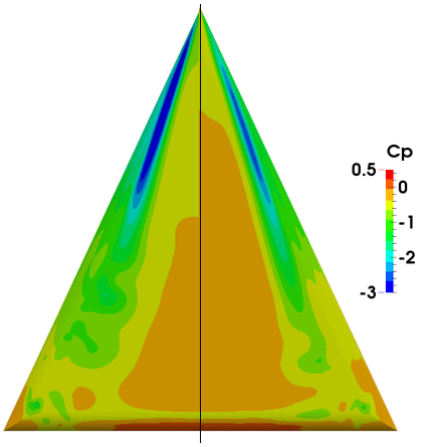

Fig. 7 Surface contours of pressure coefficient, DDES-4M-OF: $\alpha = 23°$ (left), $\alpha = 18°$ (right)

CONCLUSIONS

Two closure models (*k-w* SST and SA–DDES) are used to resolve and examine the flow around a delta wing at high angles of attack. The complex phenomenon of vortex breakdown, which is found to be best-resolved using the DDES method in OpenFOAM, is studied and commented upon. A list of all pertinent conclusions are listed below.

1. URANS models may poorly capture vortex breakdown. The present results show that it is hardly apparent that breakdown occurs, and requires further study. It may also be postulated, because of the steady nature of these models, that the spiral-mode instability would not be properly captured in any case (based on the criteria of oscillating pressure in the core, as shown in Fig. 6).
2. SA-DDES results show the formation of a bubble-like structure, which appears to be the first indication of forthcoming breakdown. This is followed by the classic spiral burst mode.
3. FLUENT results show inability to resolve a sufficient portion of turbulence necessary to produce breakdown. As the breakdown is clearly predicted in the OpenFOAM results, this phenomenon is not believed to be a deficiency of the SA-DDES model itself; rather attributable to differences in numerical methods.
4. The bubble-like structure is associated with a rise in vortex core pressure (evidenced by the increase in core pressure from Fig. 8(a) to (d)), which sharply decays axial flow momentum. As previously mentioned, this is consistent with the "stagnation point" observation made by Leibovich [8]. The decay in momentum leads to increased turbulent shearing stresses, activating the spiral burst mode.
5. A snapshot of the full onset of breakdown is captured (Fig. 5(c)). Here, axial flow momentum has decayed enough to cause a large portion of the vortex core to enter a mode of deficit in turbulent shearing stresses,

which is also associated with reversed core angular flow direction.

6. Increased normal stresses (Fig. 5(d-f)) in the breakdown region provide evidence of increased axial elongation ($\overline{(u')^2}$) and spanwise/vertical stretching ($\overline{(v')^2}$ and $\overline{(w')^2}$) of the vortex. The spanwise/vertical stretching expands the vortex (onset of bubble structure; Fig. 5(e)) and the axial elongation appears to aid in the spiral burst.
7. As angle of attack increases, the position of breakdown shifts toward the apex. This is primarily due to the positive correlation between adverse pressure gradient and angle of attack. A condition of complete stall is observed at $\alpha = 65°$.
8. It is recognized that a full analysis has not been completed. For future work, a TKE budget analysis will be performed at the location of breakdown.

ACKNOWLEDGEMENTS

An acknowledgement is extended to Benjamin Taylor for generating the grids in SolidMesh. The current OpenFOAM work is preceded by observations recorded by Choudhury [26].

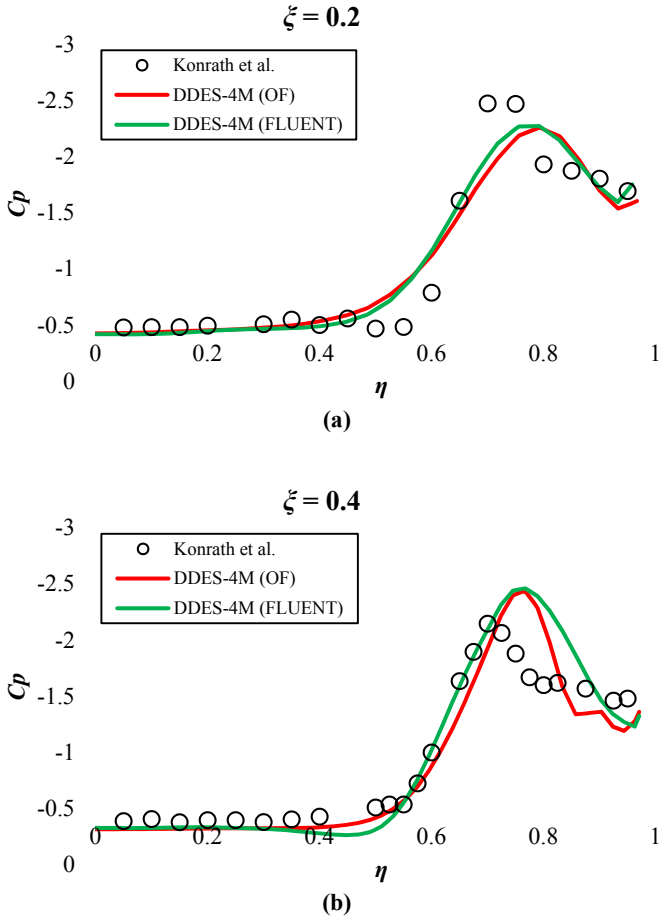

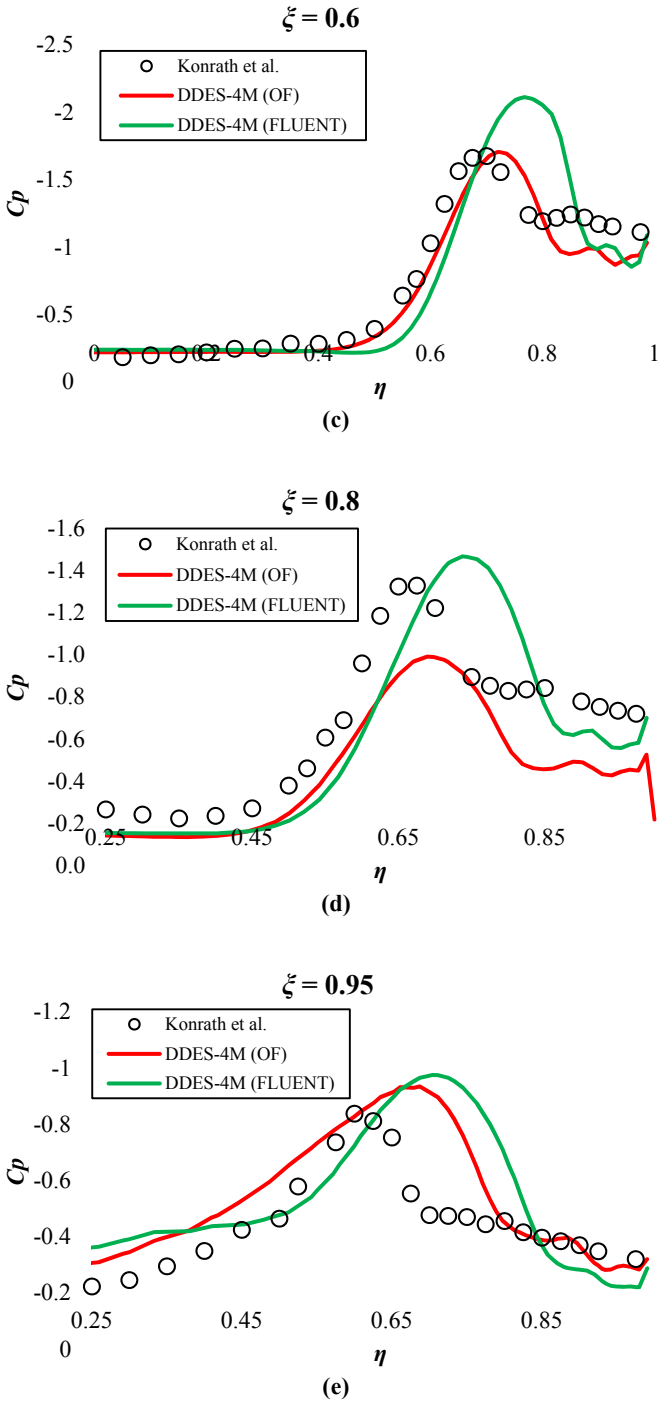

Fig. 8 Averaged pressure profiles at spanwise locations, $\alpha = 18°$: (a) ξ = 0.2, (b) ξ = 0.4, (c) ξ = 0.6, (d) ξ = 0.8, (e) ξ = 0.95.

REFERENCES

[1] Luckring, J. M., and Chu, J., 1996, "Experimental Surface Pressure Data Obtained on 65° Delta Wing Across Reynolds Number and Mach Number Ranges," NASA-TM 4645.

[2] Skow, A. M., and Erickson, G. E., 1982, "Modern Fighter Aircraft Design for High-Angle-of-Attack Maneuvering," High Angle-of-Attack Aerodynamics, AGARD-LS-121

[3] Werle, H., 1954, "Quelques Résultats Expérimentaux sur les Ailes en Fleche, aux Faibles Vitesses, Obtenus en Tunnel Hydrodynamique," La Recherche Aeronautique.

[4] Peckham, D. H., and Atkinson, S. A., 1960, "Preliminary Results of Low Speed Wind Tunnel Tests on a Gothic Wing of Aspect Ratio 1.0," Aeronautical Research Council C.P. No. 508.

[5] Elle, B. J., 1960, "On the Breakdown at High Incidences of the Leading Edge Vortices on Delta Wings," Journal of the Royal Aeronautical Society, 64(1), pp. 491.

[6] Benjamin, T. B., 1962, "Theory of the vortex breakdown phenomenon," J. Fluid Mech., 14(1), pp. 593-629.

[7] Benjamin, T. B., 1967, "Some developments in the theory of vortex breakdown," J. Fluid Mech., 28(1), pp. 65-84.

[8] Leibovich S., 1978, "The structure of vortex breakdown," Annu. Rev. Fluid Mech., 10(1), pp. 221-246.

[9] Fritz, W., 2011, "Numerical solutions for the VFE-2 configuration on structured grids at EADS-MAS," Germany

[10] Furman, A., 2013, "Turbulent and unsteady flow characteristics of delta wing vortex systems," Aerospace Science and Technology, 24(1), pp. 32-44.

[11] Cummings, R. M., and Schutte, A., 2013, "Detached-Eddy Simulation of the vortical flow field about the VFE-2 delta wing," Aerospace Science and Technology, 24(1), pp. 66-76.

[12] Luckring, J. M., and Hummel, D., 2013, "What was learned from the new VFE-2 experiments?," Aerospace Science and Technology, 24(1), pp. 77-88.

[13] SolidMesh, unstructured AFLR mesh generation and geometry system for CFD applications, Mississippi State University, http://afrl.hpc.mil/software/info/solidmesh/

[14] Menter, F., Kuntz, M., and Langtry, R., 2003, "Ten years of industrial experience with the SST turbulence model," Turbulence, heat and mass transfer, 4(1), pp. 625-32.

[15] Spalart, P. R., Deck, S., Shur, M., Squires, K., Strelets, M. K., and Travin, A., 2006, "A new version of detached-eddy simulation, resistant to ambiguous grid densities," Theoretical and computational fluid dynamics, 20(1), pp. 181-95.

[16] Spalart, P. R., and Allmaras, S. R., "A One-Equation Turbulence Model for Aerodynamic Flows," Recherche Aerospatiale, No. 1, 1994, pp. 5-21.

[17] Caruelle, B., and Ducros, F., 2003, "Detached-Eddy Simulations of Attached and Detached Boundary Layers," International Journal of Computational Fluid Dynamics, 17(6), pp. 433-451.

[18] Constantinescu, G. S., and Squires, K. D., 2003, "LES and DES investigations of turbulent flow over a sphere at Re= 10,000," Flow, Turbulence and Combustion, 70(1), pp. 267-298.

[19] Sweby, P. K., "High resolution schemes using flux limiters for hyperbolic conservation laws," SIAM J. Numer. Analysis, 21, pp. 995-1011, 1984.

[20] Issa, R. I., 1986, "Solution of the implicitly discretised fluid flow equations by operator-splitting," Journal of computational physics, 62(1), pp. 40-65.

[21] OpenFOAM®, the Open Source CFD Toolbox, Ver. 2.0.0, ESI Group, Paris, France, 2011.

[22] Jasak, H., 1996, "Error analysis and estimation for finite volume method with applications to fluid flows," PhD thesis, Imperial College, London, UK.

[23] Hunt, J. C. R., Wray, A. A., and Moin, P., 1988, "Eddies, stream, and convergence zones in turbulent flows," Center for Turbulence Research Report CTR-S88, pp. 193–208.

[24] Ludwieg, H., 1962, "Zur Erklärung der Instabilität der über angestellten Deltaflügeln auftretenden freien Wirbelkerne," Göttingen Aerodynamische Versuchsanstalt, 62(6).

[25] Konrath, R., Klein, Ch., and Schroeder, A., 2008, "PSP and PIV investigations on the VFE-2 configuration in sub- and transonic flow," AIAA Paper 2008-0379.

[26] Choudhury, V., 2013, "A Validation study of OpenFOAM for Hybrid RANS-LES simulation of Incompressible flow over a Backward Facing Step and Delta wing," Master's thesis, Mississippi State University, Starkville, MS.